Draft version October 11, 2024
Typeset using LaTeX default style in AASTeX631

Strong Photospheric Heating Indicated by Fe I 6173 Å Line Emission During White-Light Solar Flares

Samuel Granovsky,[1] Alexander G. Kosovichev,[1,2] Viacheslav M. Sadykov,[3] Graham S. Kerr,[4,5] and Joel C. Allred[5]

[1]*Department of Physics, New Jersey Institute of Technology, Newark, NJ 07102, USA*
[2]*NASA Ames Research Center, Moffett Field, Mountain View, CA 94040, USA*
[3]*Department of Physics & Astronomy, Georgia State University, Atlanta, GA 30302*
[4]*Department of Physics, Catholic University of America, 620 Michigan Avenue, Northeast, Washington, DC 20064, USA*
[5]*NASA Goddard Space Flight Center, Heliophysics Science Division, Code 671, 8800 Greenbelt Road, Greenbelt, MD 20771, USA*

ABSTRACT

Between 2017 and 2024, the Helioseismic and Magnetic Imager (HMI) onboard the Solar Dynamics Observatory has observed several white-light solar flares. Notably, for the X9.3 flare of September 6, 2017, HMI spectro-polarimetric observations reveal one or more locations within the umbra of the associated active region where the Fe I 6173 Å line goes into full emission, indicating significant heating of the photosphere and lower chromosphere. For these flares, we performed a spectro-polarimetric analysis at the aforementioned locations using HMI 90s cadence Stokes data. At the Fe I emission locations, line-core emission is observed to last for a single 90 s frame and is either concurrent with or followed by increases in the line continuum intensity lasting 90 to 180 seconds. This is followed by a smooth decay to pre-flare conditions over the next three to twenty minutes. For most locations, permanent changes to the Stokes Q, U, and/or V profiles were observed, indicating long-lasting non-transient changes to the photospheric magnetic field. These emissions coincided with local maxima in hard X-ray emission observed by the Konus instrument onboard the Wind spacecraft, as well as local maxima in the time derivative of soft X-ray emission observed by GOES satellites. Comparison of the Fe I 6173 Å line profile synthesis for the ad-hoc heating of the initial empirical VAL-S umbra model and quiescent Sun (VAL-C-like) model indicates that the Fe I 6173 Å line emission in the white-light flare kernels could be explained by the strong heating of initially cool photospheric regions.

1. INTRODUCTION

Solar flares are powerful localized electromagnetic radiation bursts in the solar atmosphere, which release vast amounts of energy across the electromagnetic spectrum. While flares are mainly associated with high X-ray and (extreme-) UV emission, certain flares are accompanied by an increase in visible continuum intensity and are thus referred to as white-light flares (WLFs). While white-light enhancement relative to the initial photospheric luminosity is typically greatest during stronger flares, WLFs have been observed as low as GOES class C1.6 (Hudson et al. 2006).

The origin of WLFs, and, in particular, the compact and short-lived WLF kernels (or cores), has been a subject of long-standing debates (see, Machado et al. 1986; Neidig 1989; Fletcher et al. 2011; Procházka et al. 2019, and references therein). Early observations showed that the WLF cores are extremely small with a characteristic size of 1.5-3 arcsec (1-2 Mm) when observed in central parts of the solar disk. Their area is less than 1% of the flare area observed for the same flares in Hα. The WLF cores are observed in the penumbra areas in the vicinity of the magnetic polarity inversion line (Švestka 1970).

Although observations from the Helioseismic and Magnetic Imager (HMI) on Solar Dynamics Observatory (Scherrer et al. 2012) showed that enhancements of the continuum in the vicinity of the Fe I 6173 Å line often identified as WLF, the intense white-light cores that should be considered as a separate phenomenon are rather rare. In the HMI data, such events can be traced in all observables, including the Doppler shift and line-of-sight magnetic field. However, due to rapid and strong variations of the line profile, the HMI 45-sec observing sequence and the inversion algorithm do not provide reliable estimates of magnetic field and plasma velocity in these events (Sadykov et al. 2020).

Spectroscopic and photometric observations suggested that the mostly likely source of the observed white-light emission is the heating of the low chromosphere and upper photosphere to high temperatures (e.g. Machado et al.

1986; Neidig 1989; Kerr & Fletcher 2014). However, explaining the WLF events in the framework of the standard thick-target flare model, which assumes the flare energy release in the form of precipitating electron beams, is faced with difficulties because the particle energy is predominantly deposited in the upper chromosphere. The radiative hydrodynamics simulations suggested that the white-light emission can be produced by free-bound hydrogen emission in a thin 'chromospheric condensation' layer formed behind the downward propagating radiative shock (Livshits et al. 1981; Kosovichev 1986; Kowalski et al. 2015), perhaps, with some contribution of radiatively heated photospheric layers (Gan et al. 2000). In addition, the radiative hydrodynamics modeling of electron beam heating with various low-energy cut-off values, E_c, using the RADYN code (Carlsson et al. 2023), showed that the electron beams with $E_c \geq 100$ keV can deposit their energy in the low chromosphere and explain the white-light emission in the Type II WLF (Procházka et al. 2019). However, the electron beams with such high low energy cut-off are not observed.

It is important to note that the WLF events observed by the HMI instrument are often accompanied by substantial rapid variations in the Fe I 6173 Å line profile, which is a deep photospheric line, and excitation of helioseismic acoustic waves ('sunquakes') (Sharykin & Kosovichev 2020). The excitation of sunquakes provides unambiguous evidence that the flare hydrodynamic impacts affect the solar photosphere and, in some cases, even the subphospheric layers on the Sun (Stefan & Kosovichev 2020; Lindsey et al. 2020; Stefan & Kosovichev 2022). The HMI observations of the X1.5 flare of May 10, 2022, which produced strong sunquakes, showed emission in the core of the Fe I 6173 Å line in the sunquake sources coinciding with the bright continuum emission cores (Kosovichev et al. 2023). The analysis of the Stokes profiles at the emission cores revealed impulsive and permanent changes in the vertical and horizontal magnetic field components, unambiguously confirming previous indications of magnetic field changes in solar flares (Zvereva & Severnyj 1970; Zirin & Tanaka 1981; Wang et al. 1994). Comparisons with the RADYN models showed that the line core emission can be explained by proton beams with the cut-off energy $E_c \geq 500$ keV, but stronger sunquake-like helioseismic impacts are provided by proton beams with $E_c \leq 100$ keV (Sadykov et al. 2024). The idea that the flare white-light emission is produced by deeply penetrating protons was suggested previously (e.g. Švestka 1970; Simnett 1986). However, a consistent model that would explain the X-ray and optical observations of the WLF cores and account for both accelerated electrons and protons, has not been developed.

In this paper, we present a spectro-polarimetric analysis of five white-light flares which took place between solar cycles 24 and 25. These flares are characterized by instances of the Fe I 6173 Å line briefly going into full emission, a phenomenon which can not be fully accounted for by the proton beam simulations studied by Kerr et al. (2023) and Sadykov et al. (2024), both of which used the plage-like atmospheres. In particular, we examine the SOL2017-09-06T11:53 X9.3 GOES-class flare which featured the greatest number and intensity of Fe I 6173 Å line emission. Every observed instance of line emission occurred above sunspot umbra, suggesting that lower photospheric temperatures may be a prerequisite, whereas the recent proton beam flare simulations had photospheric temperatures typical of the quiet Sun. To provide additional evidence for this, we performed radiative transfer modeling of the Fe I 6173 Å line for our existing proton beam simulations results, but with a modified temperature profile guided by the VAL-S umbra model and VAL-R penumbra models (Fontenla et al. 2006). This experiment reveals that photospheric temperature profiles resembling those above sunspot umbrae may lead to the Fe I 6173 Å line entering full emission. In contrast, profiles that correspond to those found above hotter sunspot penumbrae and quiet sun regions may be more likely to result in partial line core emission which does not exceed continuum intensity. While the findings are not entirely physically consistent, they suggest that lower photospheric temperatures may increase the likelihood of achieving line reversal. These experiments also demonstrate the need to perform self-consistent RADYN modelling of proton beam driven flares using realistic umbral/penumbral pre-flare stratification.

2. HMI OBSERVATIONS

The HMI instrument collects spectro-polarimetric data by capturing linear and circular polarized narrow-band images at six wavelengths across the Fe I 6173 Å line using two cameras (Couvidat et al. 2012; Schou et al. 2012). The images, with a resolution of 4096 x 4906 pixels, cover the entire disk at a sampling rate of 0.5" per pixel giving a spatial resolution of 1". Polarized images are acquired every 3.75 seconds, with the complete spectro-polarimetric measurement sequence taking 90 seconds for linear polarization and 45 seconds for circular polarization. These images are sequenced to minimize systematic errors caused by line variations during observing cycles and are then combined into the Stokes line profiles. Consequently, HMI observations deliver the full Stokes line profiles for the Fe I 6173 Å line with a spectral resolution of 68 mÅ , a spatial resolution of 1", and a temporal resolution of 90 seconds. In the standard HMI data processing pipeline, the Stokes profiles are utilized to determine the vector magnetic field and LOS velocity

through a simplified Milne–Eddington inversion procedure. However, this approach does not yield robust results for flare properties due to the rapid variations in the line profile (Švanda et al. 2018). Therefore, our focus is on analyzing the variations in the Stokes profiles at sunquake sources.

For each flare, 90 second cadence HMI Stokes image data for 13 to 15 frames (representing a time span of 19.5 to 22.5 minutes) are analyzed while ensuring immediate pre-flare and post-flare conditions are included. Due to the 90s cadence, these emission events can not be effectively resolved temporally as proton beam heating lasts for significantly shorter than this. These data are retrieved from the Joint Science Operations Center (JSOC) database. After mapping to helioprojective coordinates, the images are cropped around the flaring region and are tracked relative to the first frame in the time-series based on the local differential rotation rate to allow for temporal analysis. The Stokes I images are then normalized to pre-flare continuum intensity, and Stokes Q, U, and V are normalized to pre-flare continuum intensity for a patch of quiet sun. Pre-flare continuum intensity is approximated using the mean of filtergram channel 1 and 6 data corresponding to $\lambda_0 \pm 170$mÅ for the first image in the time-series. However, due to the low spectral sampling rate, the complex line shape within magnetized regions, and the fact that the full absorption line is not captured and often off center in HMI data, it is not possible to reliably estimate the true continuum intensity value (Švanda et al. 2018). To determine locations where the line goes into emission, line-core emission maps representing the line-core to line-wing (CtW) ratio are used. These maps are computed by dividing the mean of the two Stokes I maps corresponding to $\lambda_0 \pm 34$mÅ (channels 3 and 4) by the mean of the two Stokes I maps corresponding to $\lambda_0 \pm 170$mÅ (channels 1 and 6). Due to SDO's orbital motion and the Sun's rotation, the absolute wavelength bandpass for each filtergram channel varies over time resulting in an inconsistent CtW ratio definition relative to the true position of the line core. Due to the complex line shape, the "cropped" portion of the line wing for a significantly shifted line can not reliably be calculated to find the true average of the wings an equal distance from the line core. Therefore, the CtW ratio is not a metric which can be used to accurately compare the relative core emission strength between flares, and is instead used as an approximate method to find locations where the line goes into emission and only approximate differences in emission. For this particular set of observations, both line core absorption and emission exclusively occurs in filtergram channels 3 and 4 so the CtW ratio metric always contains the line-core within its line-core window.

Using this procedure, twenty-one flares between 2016-11-30 and 2024-03-28 with associated sunquakes from strong photospheric impacts were analyzed. Out of these twenty-one events, all featured instances of increased white-light emission, and five were found to have instances of the line going into either full emission or line core emission comparable to or exceeding line wing intensity. The five events featuring large line core emission are further discussed below. For each instance of significant line-core emission, the mean Stokes parameters of a 3x3 pixel area representing a 1.5 square arcsecond area centered on the location with a local maximum CtW ratio is used for analysis.

2.1. *SOL2017-09-06T11:53 X9.3*

Out of the flares which were investigated, the 2017-09-06 X9.3 flare exhibited the highest frequency and intensity of observed line-core emission. Visible in the CtW maps in Figure 1, the line-core emission regions sweep across the umbra of the active region. For detailed analysis, five main locations where the line goes into full emission were chosen, which are shown in Figure 1. These locations will henceforth be referred to as locations 1-5 with their helioprojective coordinates listed in Figures 2-24. The maximum CtW ratio at these locations in order are: 1.69, 1.47, 1.41, 1.78, and 1.50. Between 11:57:00 UT and 11:58:30 depending on location, the line-wings were observed to increase in brightness by between 100% and 200%, and the line-core was observed to increase in brightness by between 100% and 300% relative to pre-flare values. For locations 1, 4, and 5, transient core and wing brightening is observed in Stokes I for a single frame as the line goes into full emission. Due to the 90s sampling cadence, these emission events can not be temporally resolved. For locations 1 and 4, the line then fades to its approximate pre-flare condition over the next ten to twenty minutes. However, location 5 observations show a sustained continuum brightness which lasts for roughly five minutes before beginning to fade indicating heating was sustained for longer relative to other locations. Location 4 observations also show the line is blue-shifted by roughly half a filtergram channel (-34 mÅ or -1.6 km/s) during peak emission relative to both its pre-flare and post-flare state. For locations 2 and 3, core emission reaches its peak one frame before the line-wings, which indicates that the impact affected the upper layers of the photosphere before the lower layers. Similar to locations 1, 4, and 5, the line fades to its pre-flare condition over the next ten to twenty minutes. Stokes Q, U, and V observations for locations 1 and 3 indicate rapid changes in the magnetic field at the time of maximum emission before approaching their pre-flare conditions. However, the same observations for locations

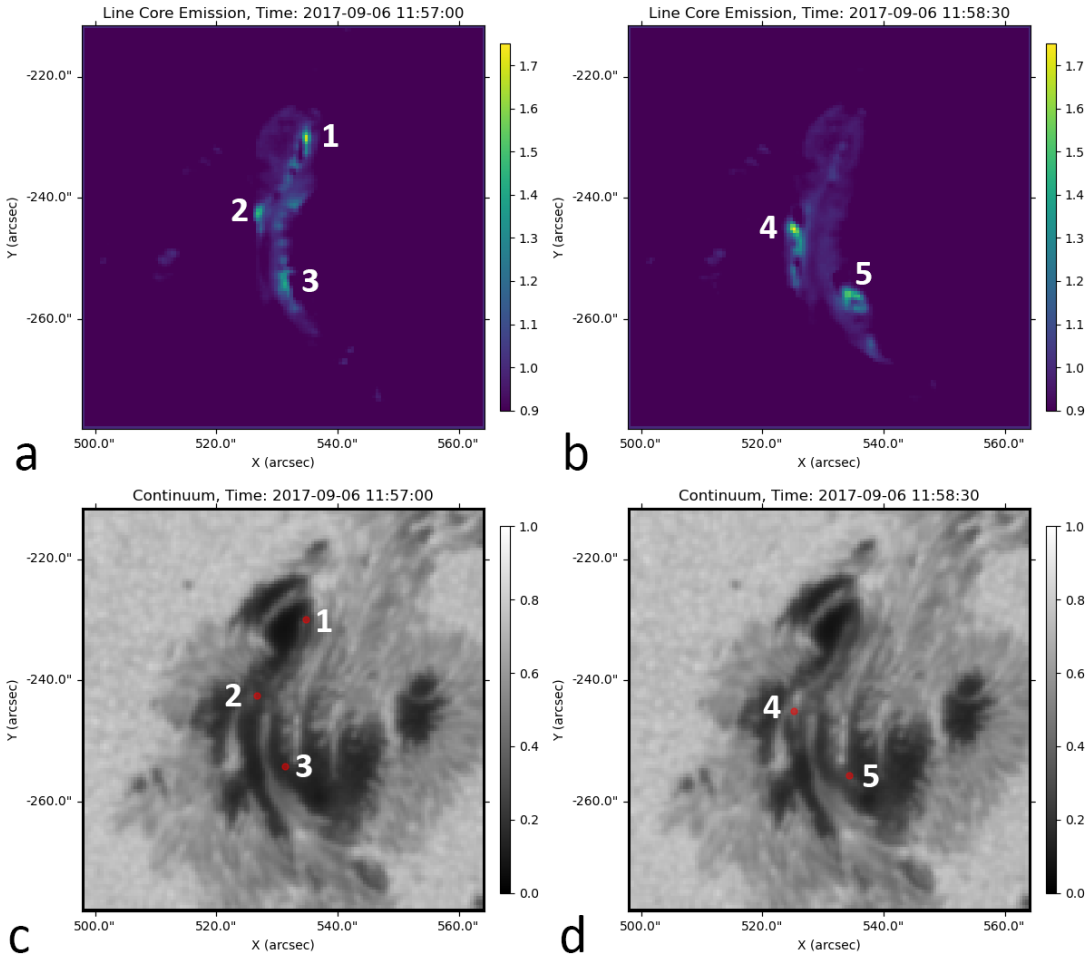

Figure 1. The Fe I 6173 Å Stokes I line-core to line-wing (CtW) ratio observed by the HMI instrument during the 2017-09-06 X9.3 flare. Panels a and b show CtW ratio during maximum emission. Points 1-5 correspond to the five locations with strongest emission whose Stokes profiles are analyzed. Panels c and d show the same locations in red on the corresponding normalized HMI continuum maps.

2, 3, and 5 indicate permanent changes to the magnetic field. Based on the KONUS-WIND hard X-ray data and the time derivative of GOES soft-X-ray data shown in Figure 8, these emissions were observed during peak hard x-ray emission.

2.2. *SOL2017-09-06T08:57 X2.2*

Similar to the 2017-09-06 X9.3 flare, emission was observed to sweep across the umbra of the active region during the 2017-09-06 X2.2 flare (figure 9). However, a CtW ratio greater than 1.1 was observed at only a single location, at 09:09:00, reaching a ratio of 1.29. At this location, both the line-core and wings are observed to increase by roughly 125% compared to pre flare conditions (figure 10). However, line-core emission reaches its peak one frame before the wings indicating the impact affected higher layers of the photosphere before the lower layers. Additionally, Stokes I decreases at a much more gradual rate when compared with the X9.3 flare data and does not reach its pre-flare state within ten minutes after the time of maximum emission. This indicates that heating lasted significantly longer when compared to the X9.3 flare. Stokes Q, U, and in particular Stokes V are permanently altered after the emission event indicating an inversion in the line of sight (LOS) magnetic field direction along with a decrease in tangential field strength. While line-core emission did not coincide with the first peak in hard X-ray emission observed by KONUS-WIND, it did coincide with the second peak in the soft X-ray time derivative observed by GOES-16 (figure 12).

2.3. *SOL2022-05-10T13:50 X1.5*

Unlike the previously discussed line-core emission events, maximum line-core emission was observed in penumbra and quiet sun regions during the 2022-05-10 X1.5 flare (figure 13). Though the maximum CtW ratio of 0.996 is relatively low, it is the greatest ratio observed on the boundary of penumbra and quiet sun out of all investigated events. Maximum line-core emission occurred at 13:55:30 with a roughly 50% increase in line-core brightness from its pre-flare condition (figure 14). The line-wings saw a roughly 30% increase in brightness from pre-flare conditions reaching its peak one frame after peak line-core emission indicating the impact affected higher layers of the photosphere before the lower layers. The line initially fades rapidly over the span of 90-180s, after which the line-wings increase in brightness and stabilize to a value roughly 15% higher compared to pre-flare conditions. Stokes Q, U, and V are all permanently altered after the emission event indicating an increase in tangential magnetic field strength and a decrease in LOS field strength (figure 14). Line-core emission appears to coincide with the first peak in hard X-ray emission observed by KONUS-WIND and the soft X-ray time derivative observed by GOES-16 (figure 16).

2.4. *SOL2023-12-31T21:36 X5.0*

During the 2023-12-31 X5.0 flare, two line-core emission events were observed within a local umbral region at 21:45:00 and 21:51:00 with CtW ratios of 1.05 and 1.08 respectively (figure 17). Unlike other investigated line-core

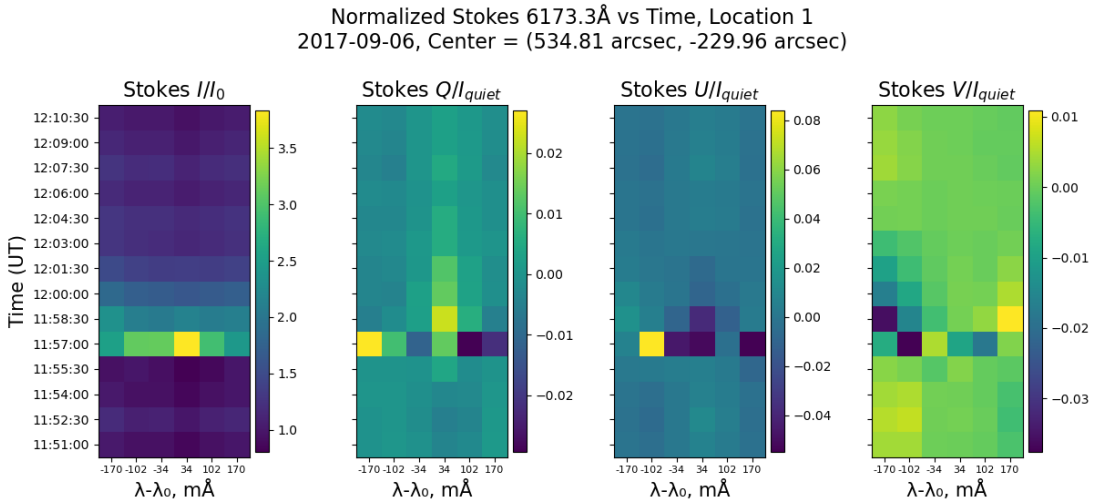

Figure 2. Fe I 6173 Å stokes parameters vs time for the 2017-09-06 X9.3 flare at location 1.

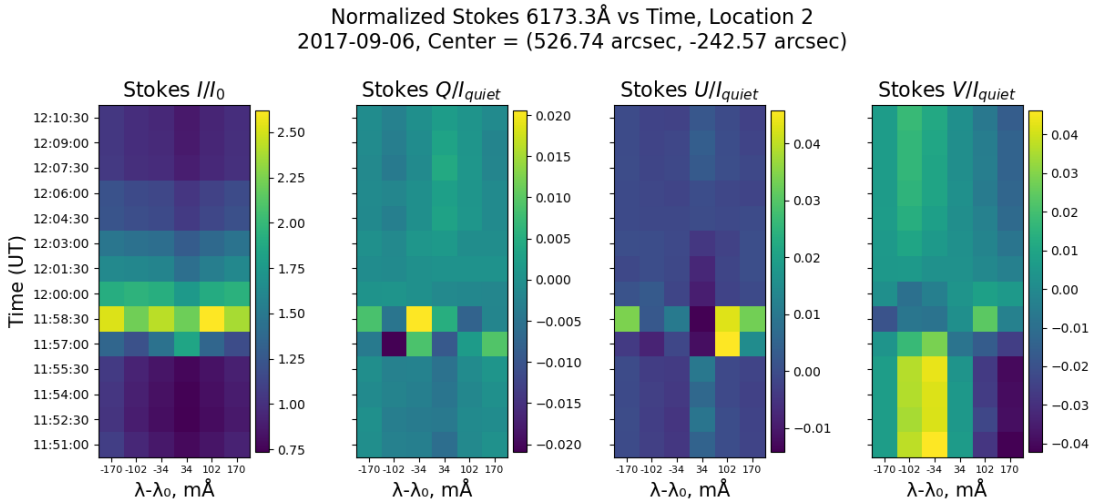

Figure 3. Fe I 6173 Å stokes parameters vs time for the 2017-09-06 X9.3 flare at location 2.

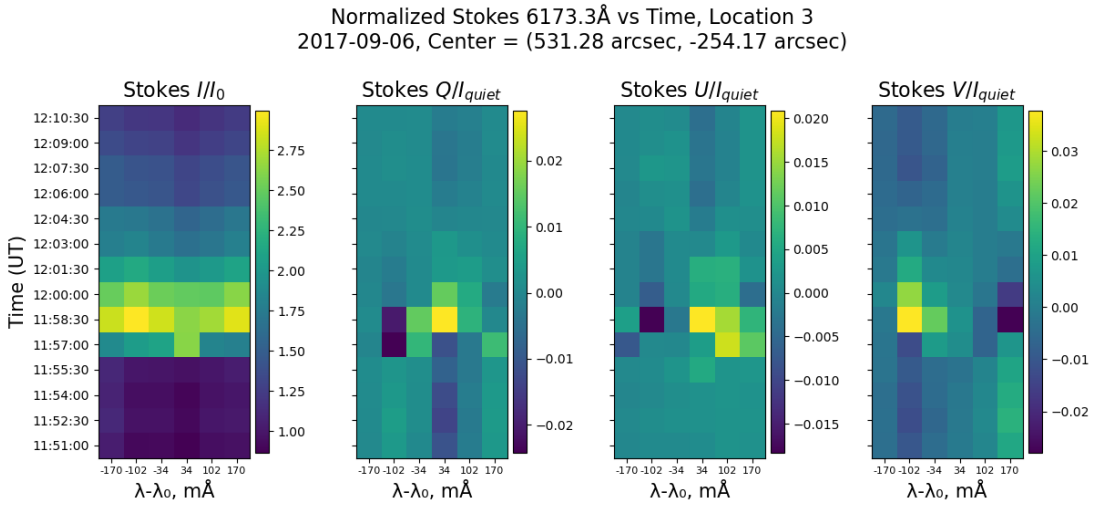

Figure 4. Fe I 6173 Å stokes parameters vs time for the 2017-09-06 X9.3 flare at location 3.

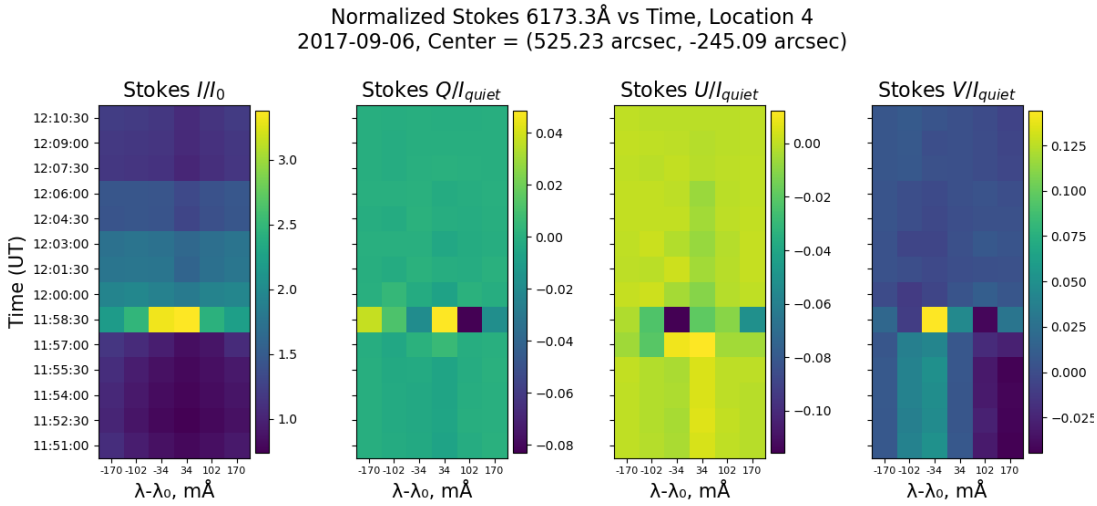

Figure 5. Fe I 6173 Å stokes parameters vs time for the 2017-09-06 X9.3 flare at location 4.

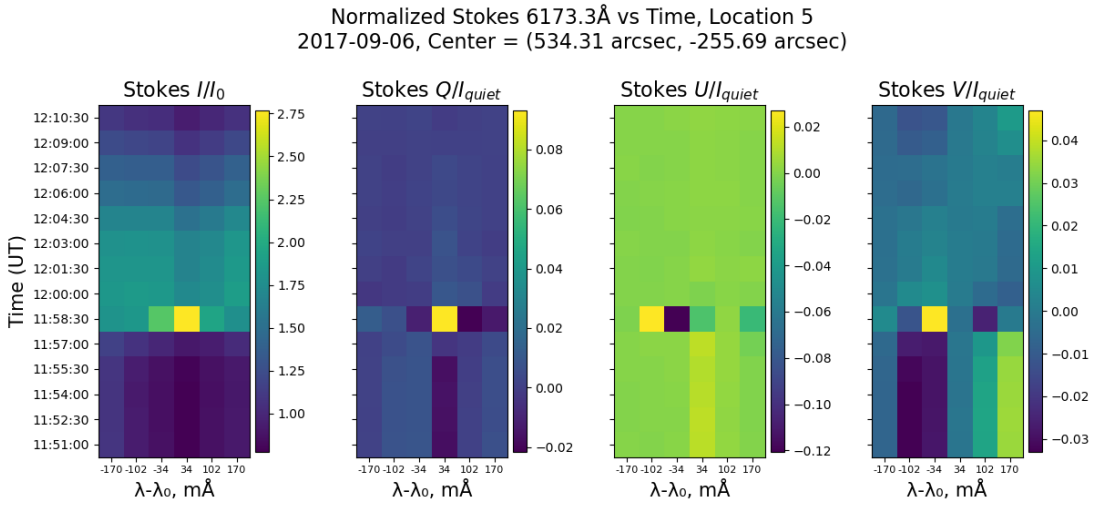

Figure 6. Fe I 6173 Å stokes parameters vs time for the 2017-09-06 X9.3 flare at location 5.

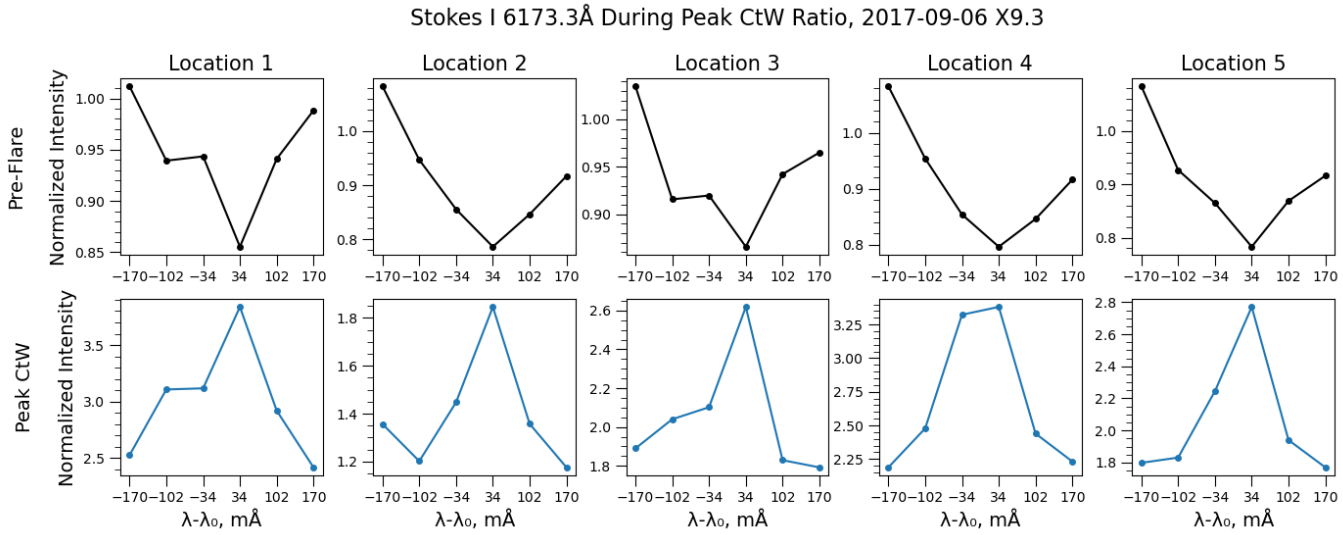

Figure 7. Fe I 6173 Å stokes I during pre-flare (top row) and during maximum CtW (bottom row) for locations 1-5 for the 2017-09-06 X9.3 flare. Intensity is normalized relative to the mean wing intensity (filtergram channels 1 and 6)

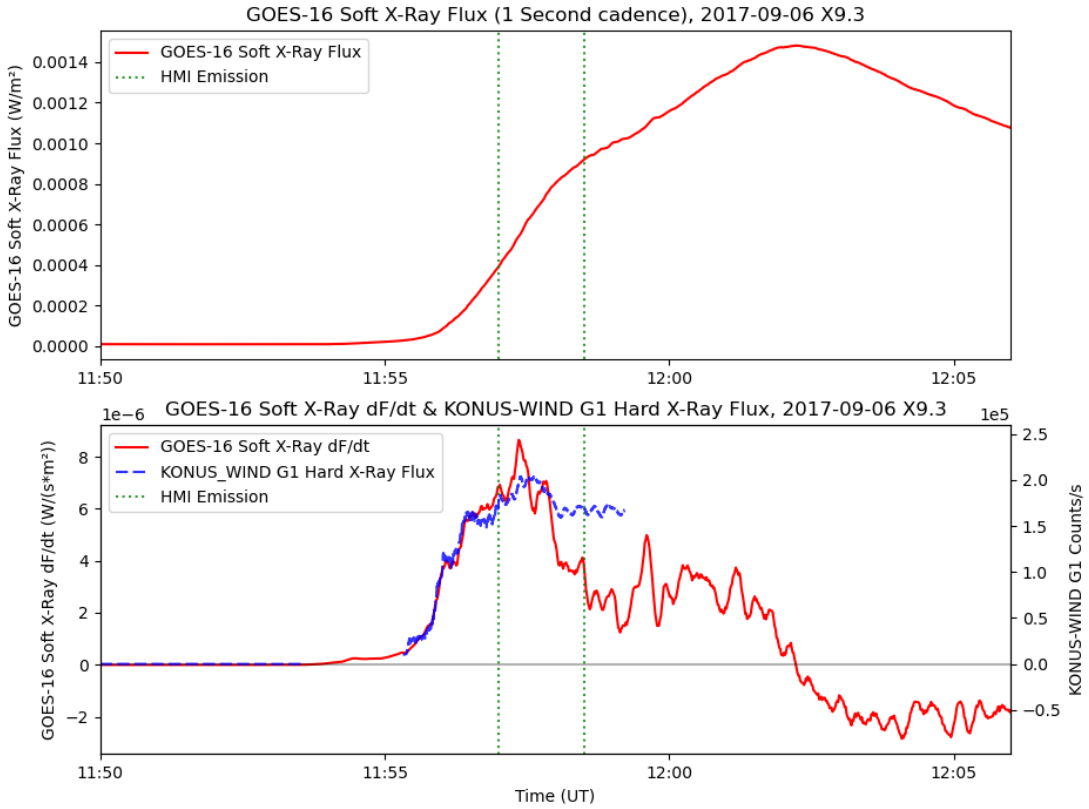

Figure 8. GOES-16 Long Soft X-ray Flux (1.55 - 12.4 keV, top panel, solid red), the time derivative of GOES-16 Long Soft X-ray Flux (bottom panel, solid red), and KONUS-WIND channel G1 Hard X-ray (17.8 keV - 75.1 keV, bottom panel, dashed blue) during the 2017-09-06 X9.3 flare. Highlighted are the times HMI observed the Fe I 6173 Å line in emission (dotted green). The X-ray curves are smoothed using a Savitzky–Golay filter.

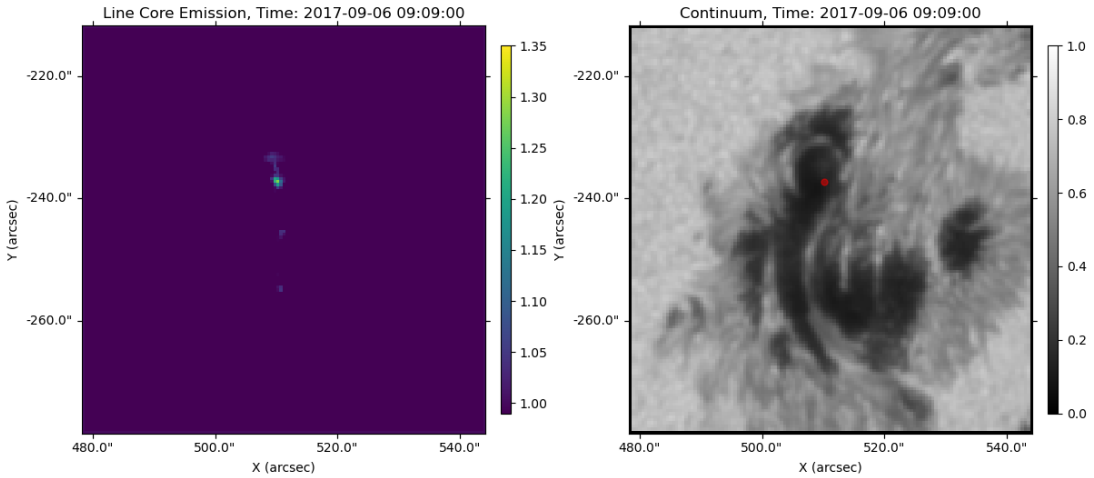

Figure 9. The Fe I 6173 Å Stokes I line CtW ratio observed by the HMI instrument during the 2017-09-06 X2.2 flare. The left panel shows CtW ratio during maximum emission. The right panel shows the corresponding normalized HMI continuum map with the maximum observed CtW location indicated by the red dot.

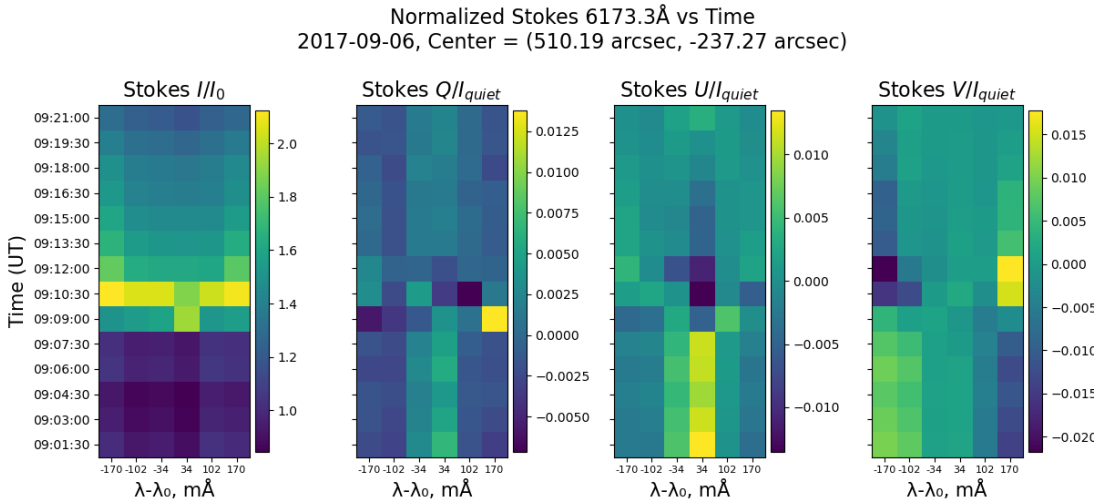

Figure 10. Fe I 6173 Å stokes parameters vs time for the 2017-09-06 X2.2 flare at the location of maximum CtW ratio.

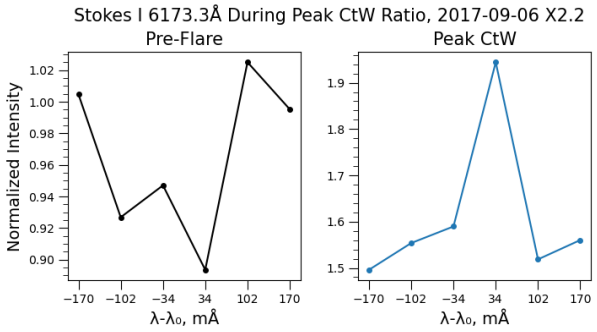

Figure 11. Fe I 6173 Å stokes I during pre-flare (left) and during maximum CtW (right) for the 2017-09-06 X2.2 flare. Intensity is normalized relative to the mean wing intensity (filtergram channels 1 and 6)

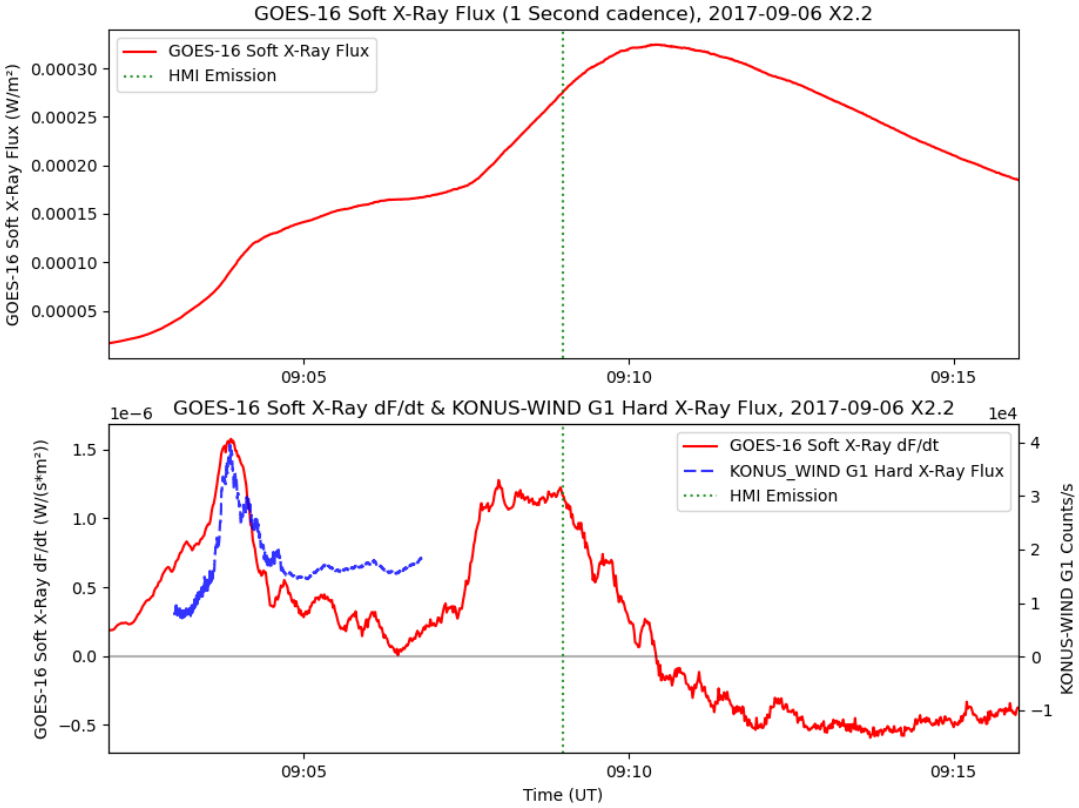

Figure 12. Same as Figure 8 for the 2017-09-06 X2.2 flare

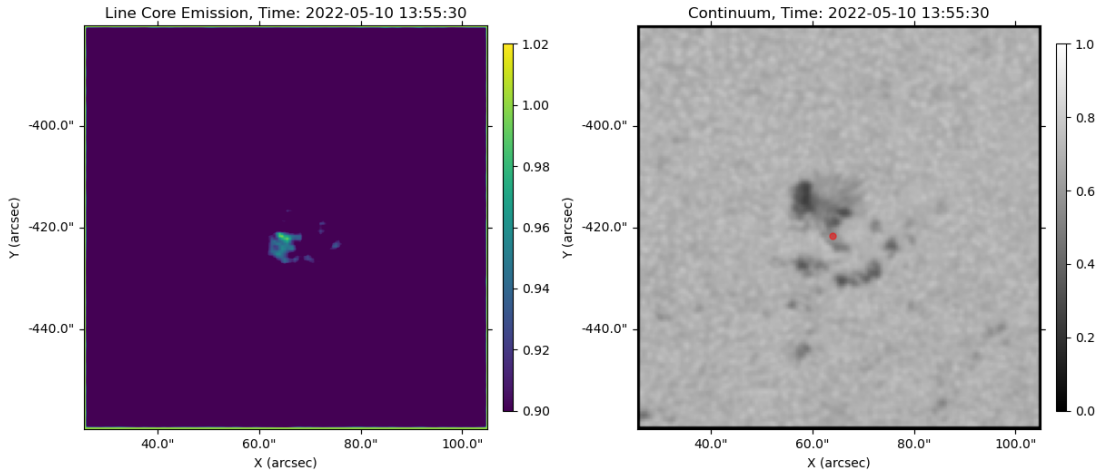

Figure 13. The Fe I 6173 Å Stokes I line CtW ratio observed by the HMI instrument during the 2022-05-10 X1.5 flare. The left panel shows CtW ratio during maximum emission. The right panel shows the corresponding normalized HMI continuum map with the maximum observed CtW location indicated by the red dot.

emission events, observations were taken close to the solar limb, so optical depth potentially affects the data. The initial 80% increase in line-core emission at 21:45:00 occurs for a single frame and coincides with a 35% increase in line-wing brightness which lasts for two frames before briefly fading over the next two frames (figure 18). At 21:51:00, a second 65% increase in line-core emission is observed 1.15 arcsec north east from the location of the 21:45:00 line-core emission.This line-core emission also lasts for a single frame and coincides with a 25% increase in line-wing brightness which lasts for 3 frames before fading (figure 19). This heating affects the line at the first location and results in an

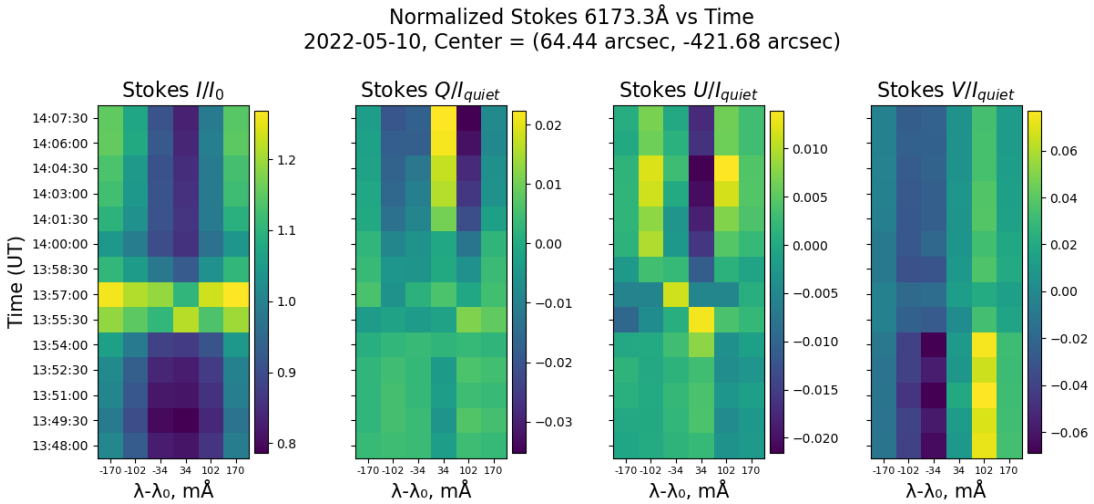

Figure 14. Fe I 6173 Å stokes parameters vs time for the 2022-05-10 X1.5 flare at the location of maximum CtW ratio.

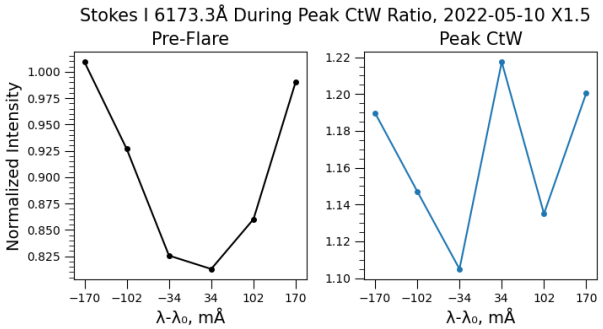

Figure 15. Fe I 6173 Å stokes I during pre-flare (left) and during maximum CtW (right) for the 2022-05-10 X1.5 flare. Intensity is normalized relative to the mean wing intensity (filtergram channels 1 and 6)

increase in the line-wings to similar intensity as during the frame following maximum CtW, however there is only a small partial line core emission 18). Stokes Q, U, and Stokes V are permanently altered after the first emission event indicating a significant weakening in both LOS and tangential magnetic field strength with the direction of the LOS field being inverted. During the second emission event, Stokes Q and V are temporarily strengthened before returning towards their values before the second emission event. KONUS-WIND hard X-ray data is not available for this flare, and though the second line-core emission appears to coincide with the peak in the soft X-ray time derivative observed by GOES-18, the first emission event occurs well before the peak estimated hard X-ray emission (figure 21).

2.5. *SOL2024-02-22T22:08 X6.3*

During the 2024-02-22 X6.3 flare, line-core emission was observed within the umbra of the associated active region at 22:30:00 with a maximum CtW ratio of 1.06. (figure 22). At this time, line-core brightness increased by roughly 65% (figure 23). The line-wings saw a roughly 60% increase in brightness from pre-flare conditions reaching its peak one frame after peak line-core emission indicating the impact affected higher layers of the photosphere before the lower layers. After peak line-wing emission, the line gradually fades and does not reach pre-flare conditions within ten minutes indicating heating lasted for longer than what was observed for most other investigated events. Stokes Q and V appear to be altered only temporarily with Stokes U demonstrating a more permanent weakening of the tangential magnetic field (figure 23). Line-core emission appears to occur just before the peak in hard X-ray emission observed by KONUS-WIND and the soft X-ray time derivative observed by GOES-16 (figure 25).

3. SEMI-EMPIRICAL RADIATIVE TRANSFER MODELING OF COLDER ATMOSPHERES

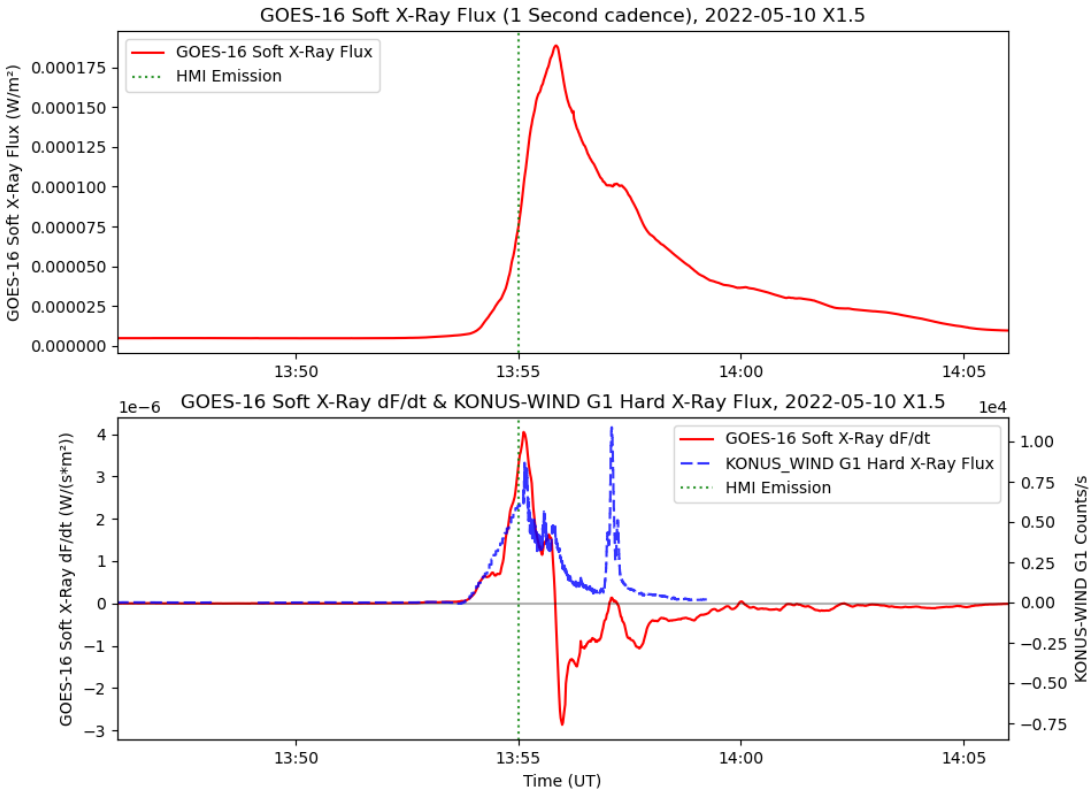

Figure 16. Same as Figure 8 for the 2022-05-10 X1.5 flare

The common denominator behind the observed line profile reversals is that they happen within sunspot umbra or penumbra. There, the photosphere is cooler in comparison with the typical quiet Sun atmospheres, and the intensity of the continuum near the SDO/HMI Fe I 6173 Å line profile is weaker. The question is to what extent such initial condition of the atmosphere favors the development of the Fe I line profile reversal.

While there are many radiative hydrodynamic simulations of the heating of the solar atmosphere by electron or proton beams (e.g. Allred et al. 2005, 2015; Kerr et al. 2023; Carlsson et al. 2023), the stratification of the initial atmospheres is mostly quiescent Sun or plage-like. There have been few studies of the impact of the pre-flare stratification on the resulting emission (e.g., Hong et al. 2018; Polito et al. 2018). An accurate modeling of the beam impact on the umbra- and penumbra-like atmosphere requires the development of a radiatively stable initial atmosphere with a temperature and mass density structure resembling umbra or penumbra semi-empirical models (for example, VAL-S and VAL-R, Fontenla et al. 2006). The development of such initial atmospheres requires a significant effort (due in part to having to account for density depletion and molecular opacities) and is out of the scope of the current paper. Instead, in this work we perform some experiments where we introduce ad-hoc temperature modifications for the existing proton beam simulation solutions (Kerr et al. 2023; Sadykov et al. 2024). While not representing self-consistent temperature evolutions (e.g. radiative heating and cooling, mass motions, height-dependent particle beam energy losses are not considered) in our ad-hoc atmospheres) , we do this to gain a qualitative understanding of how the Fe I line profile changes with the change of the initial temperature profile, $T(h)$. Here is our strategy to do this:

- Consider a proton beam heating model produced with the radiative hydrodynamics code RADYN (Allred et al. 2015, 2020; Kerr et al. 2023) and analyzed previously by Sadykov et al. (2024) where the Fe I 6173 Å line profile core demonstrated the strongest emission signatures, yet not leading to a reversal. This model has spectral energy index of $\delta = 3$, a high low cutoff energy of $E_c = 3$ MeV, and a total energy flux density of $1 \cdot 10^{11}$ erg s^{-1} cm^{-2}. The smallest ratio of the line profile depth (defined as the difference between the intensity of the continuum near the line and the smallest intensity along the line) to the continuum intensity near the line was approaching ∼0.14 for this model (see Table 1 in Sadykov et al. 2024), almost leading to the line profile reversal;

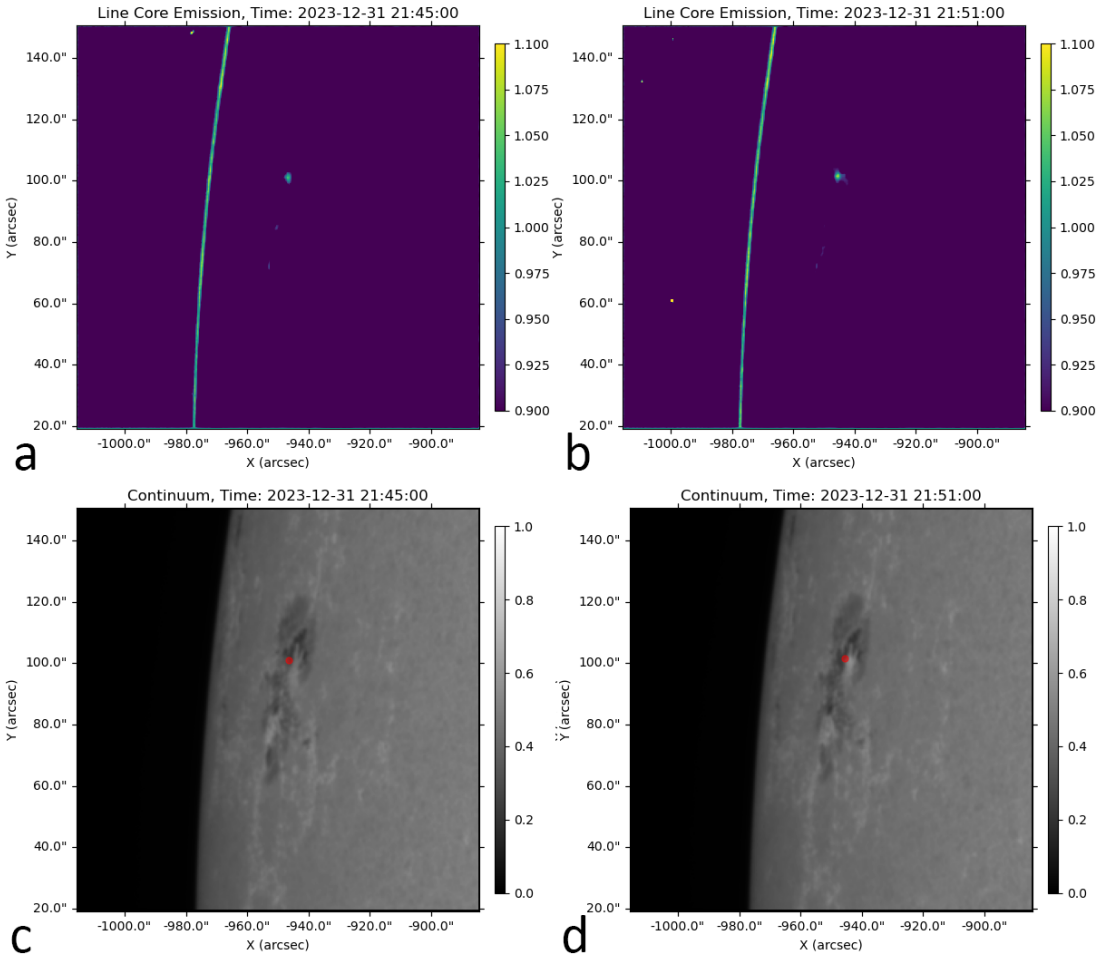

Figure 17. The Fe I 6173 Å Stokes I line CtW ratio observed by the HMI instrument during the 2023-12-31 X5.0 flare. Panels a and b show CtW ratio during maximum emission. Panels c and d show the locations of maximum CtW ratio in red on the corresponding normalized HMI continuum maps.

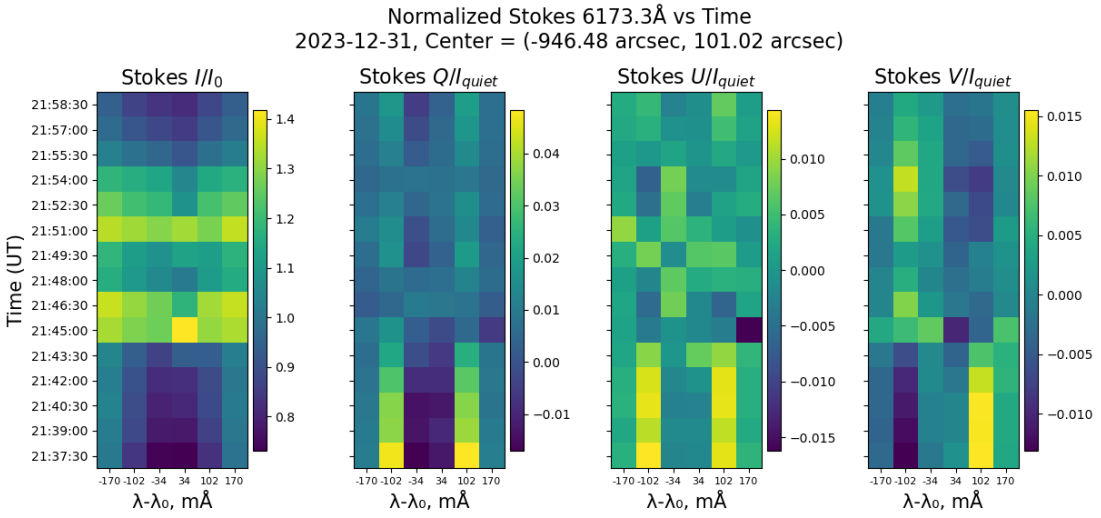

Figure 18. Fe I 6173 Å stokes parameters vs time for the 2023-12-31 X5.0 flare at the location of maximum CtW ratio at t=21:45:00.

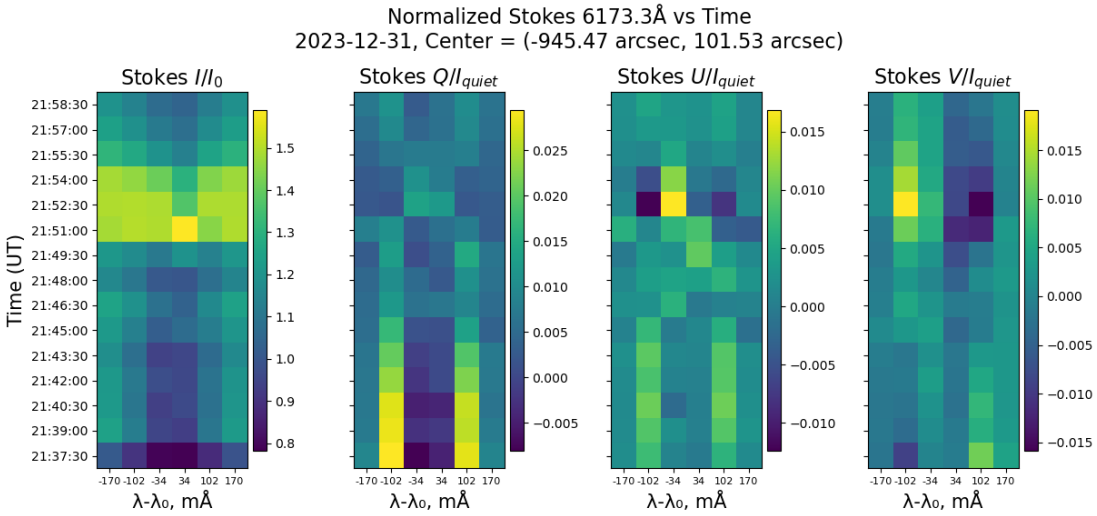

Figure 19. Same as Figure 18 at t=21:51:00.

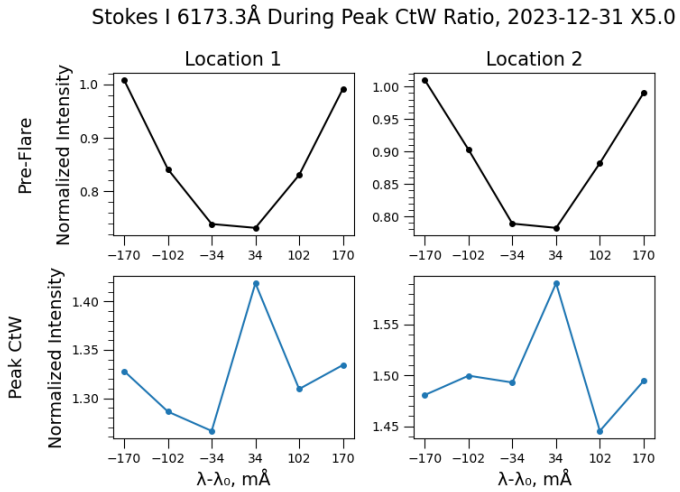

Figure 20. Fe I 6173 Å stokes I during pre-flare (top row) and during maximum CtW (bottom row) for locations 1 and 2 for the 2023-12-31 X5.0 flare. Intensity is normalized relative to the mean wing intensity (filtergram channels 1 and 6)

- Modify the temperature structure $T(h)$ of the initial atmosphere (at t=0 s) to match the temperature profile $T(h)$ of the VAL-S or VAL-R model within $z = [-50 - 420]$ km and perform a linear transition to the modelled temperature at $z = [420 - 1500]$ km. Record the corresponding $\Delta T(h)$ change as a function of height;

- Adjust all the following time steps of the model when the flare begins by the same $\Delta T(h)$ without changing the other atmospheric parameters (such as densities or bulk gas velocity). Note that the changes will apply only to the -50-1500 km portion of the atmosphere;

- Compute the Fe I 6173 Å line profiles for each time step by assuming statistical equilibrium conditions for H, Fe, and other species and free electrons and no presence of an external magnetic field.

While this approach is indeed not self-consistent, it provides a possibility to qualitatively investigate how would Fe I 6173 Å line react to the presence of the colder atmospheric temperatures while keeping all other parameters fixed. Thus, we can determine if the emission features result in atmospheres with deep heating and a smaller background radiation field than. The results are presented in Figure 26 which demonstrates the line profile at different snapshots of the original model (top row) and of the model where the temperature was adjusted to be colder according to VAL-S

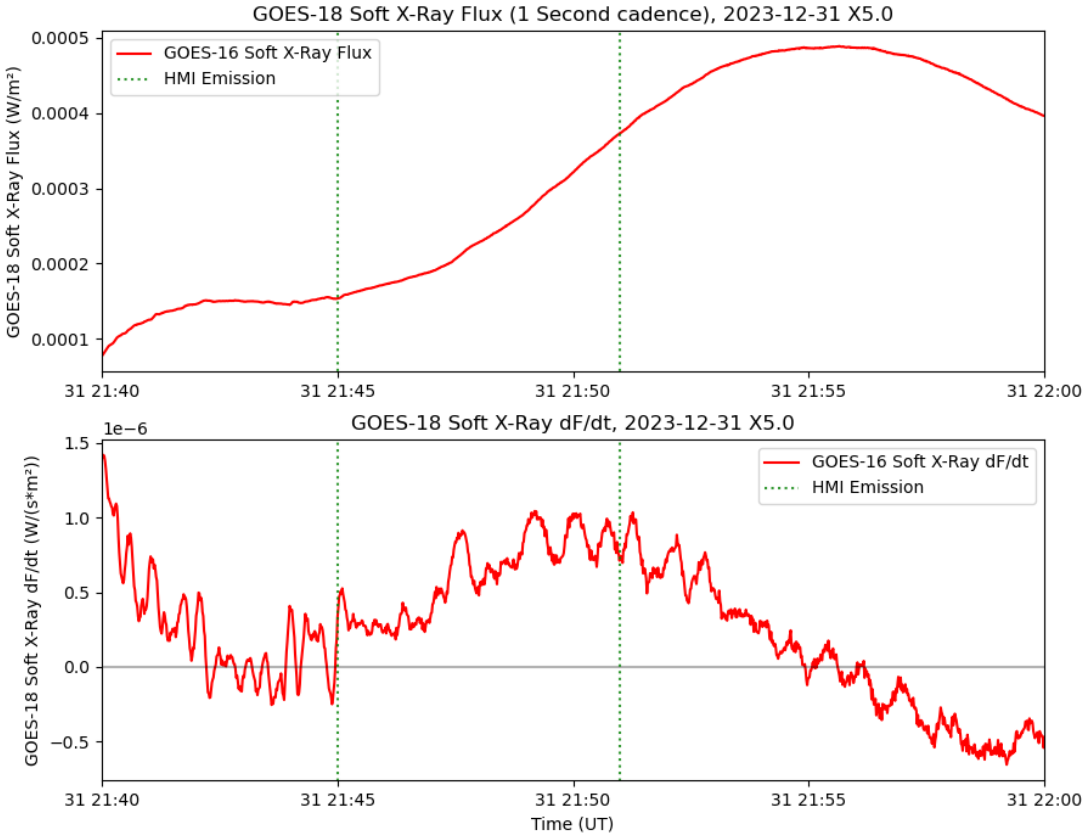

Figure 21. Same as Figure 8 for the 2023-12-31 X5.0 flare

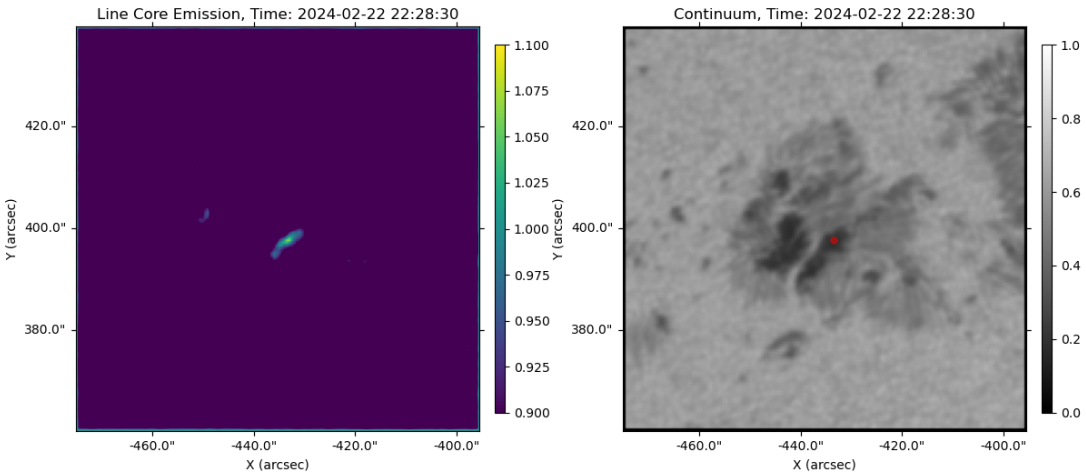

Figure 22. The Fe I 6173 Å Stokes I line CtW ratio observed by the HMI instrument during the 2024-02-22 X6.3 flare. The left panel shows CtW ratio during maximum emission. The right panel shows the corresponding normalized HMI continuum map with the maximum observed CtW location indicated by the red dot.

and VAL-R atmospheres. Overall, the temperature vs height parameter has the greatest influence on the shape of the Stokes I line profile, with lower temperatures above the photosphere consistently resulting in greater line-core emission, with the adjustments based on VAL-S resulting in the line going into full emission. Meanwhile, the model based on VAL-R featuring slightly higher temperatures within the range of optical depth heights results in less line-core emission. These results qualitatively suggest that the decreased atmospheric temperature in the lower photosphere

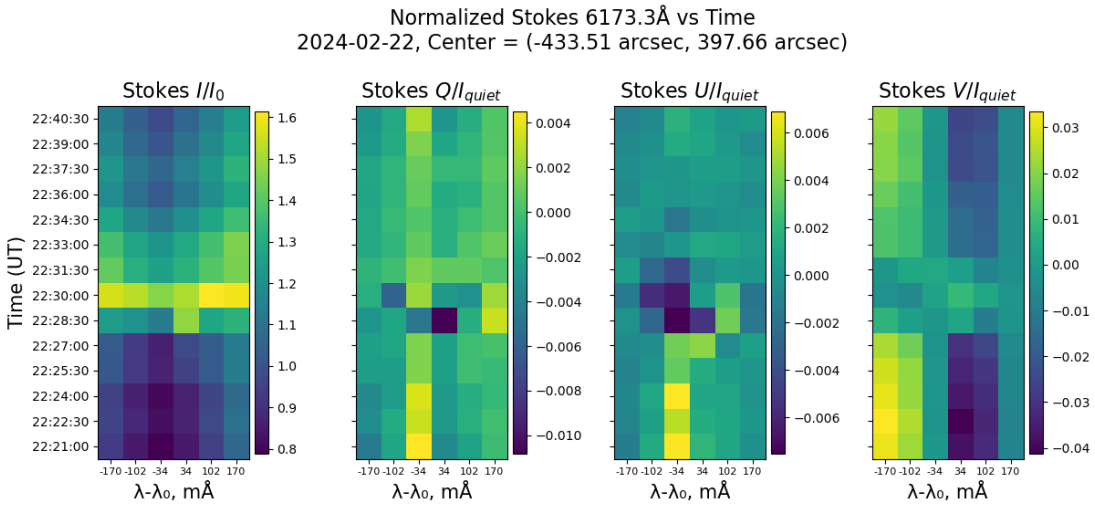

Figure 23. Fe I 6173 Å stokes parameters vs time for the 2024-02-22 X6.3 flare at the location of maximum CtW ratio.

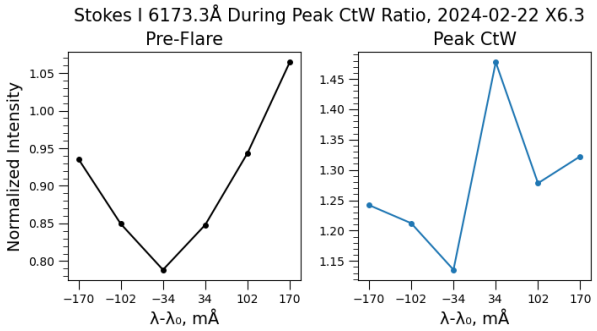

Figure 24. Fe I 6173 Å stokes I during pre-flare (left) and during maximum CtW (right) for the 2024-02-22 X6.3 flare. Intensity is normalized relative to the mean wing intensity (filtergram channels 1 and 6)

could potentially favor the reversal of the Fe I line profile. Whether such reversals are exclusive to sunspot umbras or if they could appear in more quiescent Sun-like atmospheric stratification by proton and electron beams of stronger energy fluxes remains to be seen, and will be a subject of future investigations.

4. DISCUSSION AND CONCLUSIONS

This study presents a detailed spectro-polarimetric analysis of Fe I 6173 Å line emission during five WLFs observed by SDO HMI between 2017 and 2024. Investigation of these flare events reveals that Fe I 6173 Å line emission is significantly more likely to occur above sunspot umbrae. For each flare event, a 19.5 to 22.5 minute time-series of 90 second cadence HMI Stokes data is compiled while accounting for differential rotation effects to allow for temporal analysis. Of the investigated flares, the SOL2017-09-06T11:53 X9.3 flare exhibits the highest frequency and intensity of observed line emission with the line core-to-wing ratio reaching as high as 1.78. Meanwhile, the strongest observed line-core emission above penumbral or quiet sun regions out of the investigated events, observed during the 2022-05-10 X1.5 flare, has a relatively small core-to-wing ratio of 0.996. Line core emission consistently lasts for a single 90s frame and is either concurrent with or delayed by one frame relative to continuum brightening. In cases with delayed continuum brightening, the associated flare photospheric impact affects higher layers of the photosphere first. However, due to the 90s sampling cadence, line emission can often not be temporally resolved from continuum emission and may appear simultaneous. Following the emission event, continuum intensity fades towards its pre-flare state over the next three to twenty minutes depending on the duration of heating. Lasting changes to Stokes Q, U, and or V were observed for all emission events indicating permanent changes in the magnetic field at these locations. These emissions coincided with local maxima in hard X-ray emission observed by Konus-Wind along with local maxima in the time

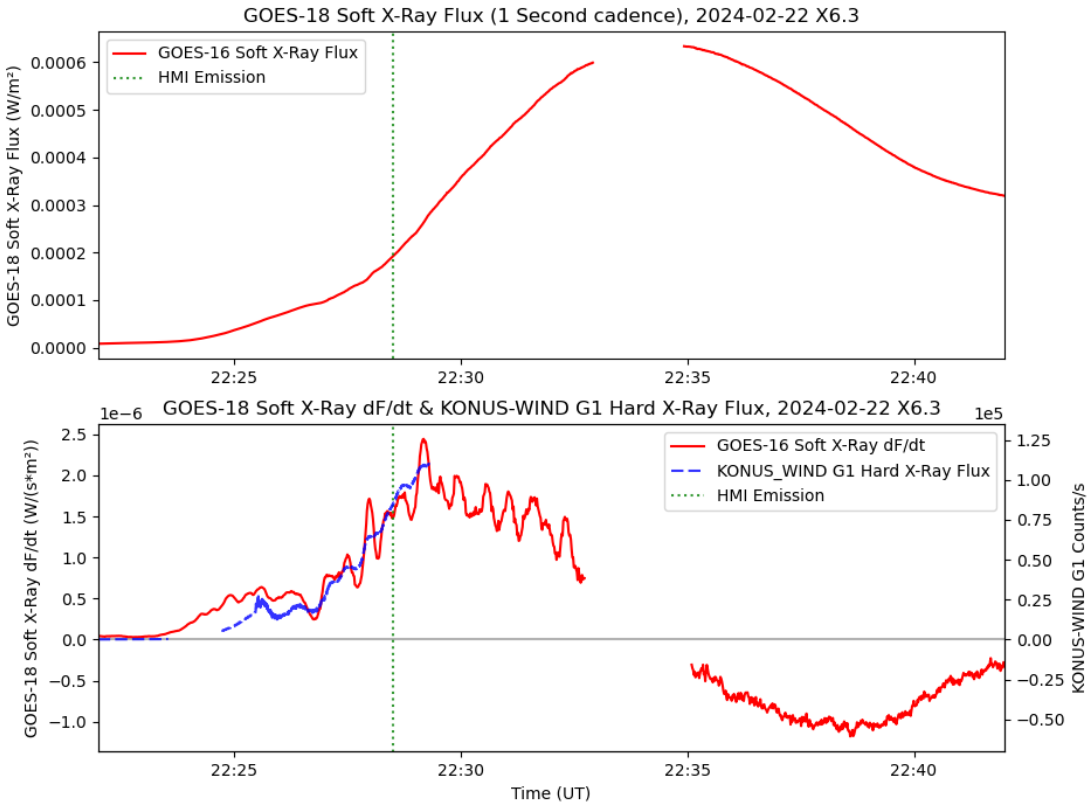

Figure 25. Same as Figure 8 for the 2024-02-22 X6.3 flare

derivative of soft X-ray emission observed by GOES satellites, suggesting the line core emissions may be concurrent with the electron beam precipitation. Again, due to the 90s sampling cadence, it is difficult to state the exact relative timing of the two events. From the frequency and intensity of line emission above sunspot umbrae relative to other regions, we conclude that cooler photospheric temperatures may promote line-core emission.

To test to what extent cooler photospheric temperatures result in increased line-core emission, we perform semi-empirical radiative transfer modeling of the Fe I 6173 Å line. This is done by modifying an existing plage-like RADYN proton beam driven flare simulation. Using modified temperature profiles corresponding to the VAL-S umbra model and VAL-R penumbra model at the initial time step of the simulation, the temperature evolution of the RADYN flare was changed whilst keeping other atmospheric properties fixed. While the original quiet sun and penumbra models feature only partial line core emission, the results indicate that umbral photospheric temperatures result in full reversal of the Fe I 6173 Å line. While these penumbral and umbral models are physically inconsistent, they demonstrate that lowering photospheric temperatures while maintaining other parameters may result in more favorable conditions for Fe I 6173 Å line reversal during proton beam impacts. This motivates the construction of penumbral and umbral models to model these features more self-consistently. Those future simulations can be used to confirm the hypothesis that we present in this manuscript. Our study also demonstrates that the underlying pre-flare atmosphere is a key factor when performing model-data comparisons.

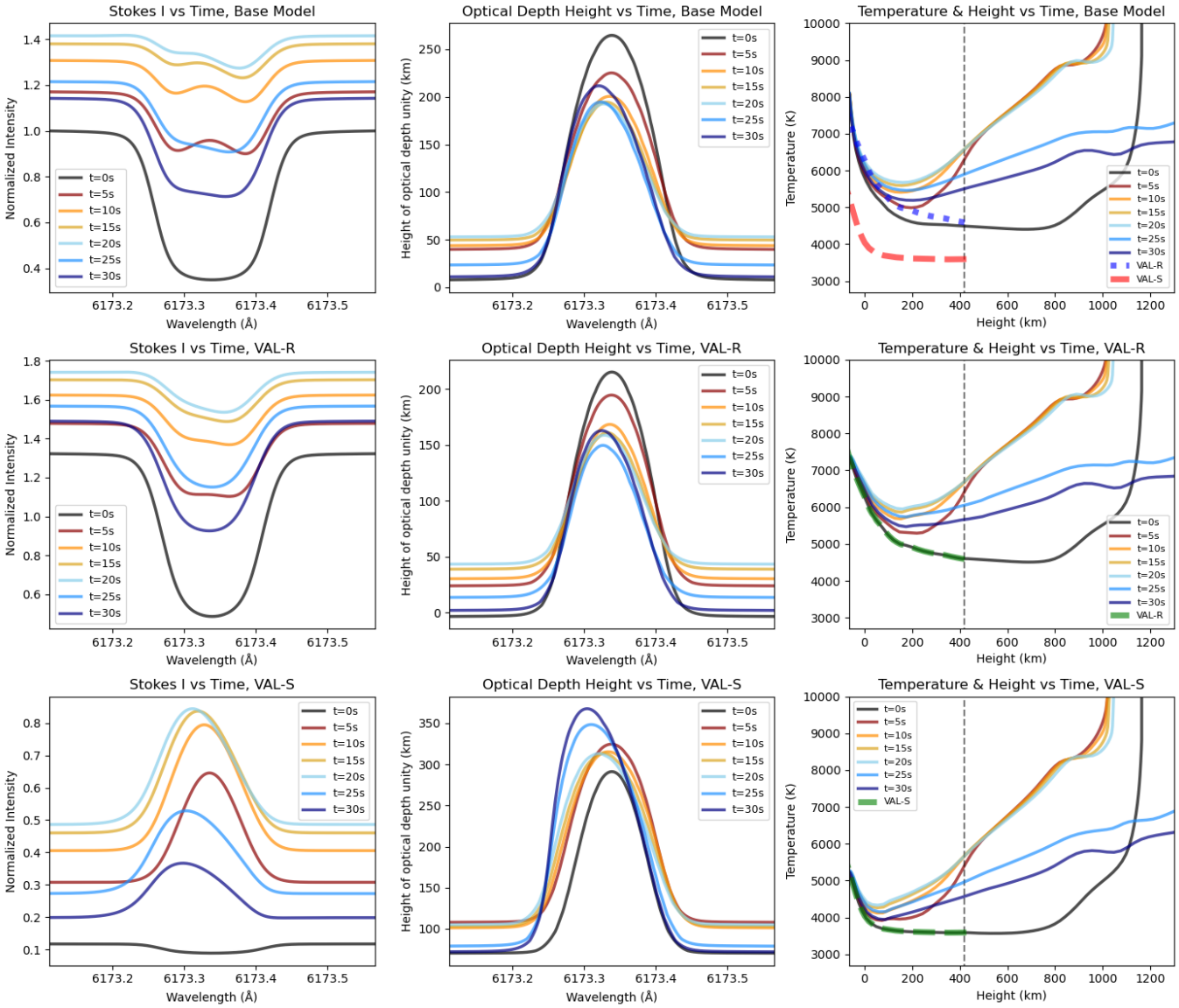

Figure 26. Synthetic Fe I 6173 Å Stokes I vs time (left), optical depth height vs time (middle), and temperature vs height vs time (right). The top row shows results from the base RADYN proton beam simulation with a typical energy flux of 10^{11} erg cm^{-2} s^{-1}, a spectral energy index of $\delta = 3$, a low cutoff energy of $E_c = 3$ MeV, and 20s proton beam heating. In addition, the VAL-R (dotted, blue) and VAL-S (dashed red) are shown. The middle row shows the result of modifying the base model to match the VAL-R temperature profile (dashed, green), and the bottom row shows the same as the middle row for the VAL-S model (dashed, green). In the temperature vs height vs time plots, all values to the left of the vertical black line have been modified such that the t=0 profile matches the VAL-R and VAL-S models, and values to the right are a linear transition from the VAL models to the base RADYN simulation. Stokes I normalization is relative to continuum intensity at t=0 in the base model results.

REFERENCES

Allred, J. C., Alaoui, M., Kowalski, A. F., & Kerr, G. S. 2020, ApJ, 902, 16, doi: 10.3847/1538-4357/abb239

Allred, J. C., Hawley, S. L., Abbett, W. P., & Carlsson, M. 2005, ApJ, 630, 573, doi: 10.1086/431751

Allred, J. C., Kowalski, A. F., & Carlsson, M. 2015, ApJ, 809, 104, doi: 10.1088/0004-637X/809/1/104

Carlsson, M., Fletcher, L., Allred, J., et al. 2023, A&A, 673, A150, doi: 10.1051/0004-6361/202346087

Couvidat, S., Schou, J., Shine, R. A., et al. 2012, SoPh, 275, 285, doi: 10.1007/s11207-011-9723-8

Fletcher, L., Dennis, B. R., Hudson, H. S., et al. 2011, SSRv, 159, 19, doi: 10.1007/s11214-010-9701-8

Fontenla, J. M., Avrett, E., Thuillier, G., & Harder, J. 2006, ApJ, 639, 441, doi: 10.1086/499345

Gan, W. Q., Hénoux, J. C., & Fang, C. 2000, A&A, 354, 691

Hong, J., Ding, M. D., Li, Y., & Carlsson, M. 2018, ApJL, 857, L2, doi: 10.3847/2041-8213/aab9aa

Hudson, H. S., Wolfson, C. J., & Metcalf, T. R. 2006, SoPh, 234, 79, doi: 10.1007/s11207-006-0056-y

Kerr, G. S., Allred, J. C., Kowalski, A. F., et al. 2023, ApJ, 945, 118, doi: 10.3847/1538-4357/acb92a

Kerr, G. S., & Fletcher, L. 2014, ApJ, 783, 98, doi: 10.1088/0004-637X/783/2/98

Kosovichev, A. G. 1986, Bulletin Crimean Astrophysical Observatory, 75, 6

Kosovichev, A. G., Sadykov, V. M., & Stefan, J. T. 2023, ApJ, 958, 160, doi: 10.3847/1538-4357/acf9eb

Kowalski, A. F., Hawley, S. L., Carlsson, M., et al. 2015, SoPh, 290, 3487, doi: 10.1007/s11207-015-0708-x

Lindsey, C., Buitrago-Casas, J. C., Martínez Oliveros, J. C., et al. 2020, ApJL, 901, L9, doi: 10.3847/2041-8213/abad2a

Livshits, M. A., Badalian, O. G., Kosovichev, A. G., & Katsova, M. M. 1981, SoPh, 73, 269, doi: 10.1007/BF00151682

Machado, M. E., Avrett, E. H., Falciani, R., et al. 1986, in The Lower Atmosphere of Solar Flares, ed. D. F. Neidig & M. E. Machado, 483–488. https://ui.adsabs.harvard.edu/abs/1986lasf.conf..483M

Neidig, D. F. 1989, SoPh, 121, 261, doi: 10.1007/BF00161699

Polito, V., Testa, P., Allred, J., et al. 2018, ApJ, 856, 178, doi: 10.3847/1538-4357/aab49e

Procházka, O., Reid, A., & Mathioudakis, M. 2019, ApJ, 882, 97, doi: 10.3847/1538-4357/ab35e1

Sadykov, V. M., Kosovichev, A. G., Kitiashvili, I. N., & Kerr, G. S. 2020, ApJ, 893, 24, doi: 10.3847/1538-4357/ab7b6a

Sadykov, V. M., Stefan, J. T., Kosovichev, A. G., et al. 2024, ApJ, 960, 80, doi: 10.3847/1538-4357/ad0cf3

Scherrer, P. H., Schou, J., Bush, R. I., et al. 2012, SoPh, 275, 207, doi: 10.1007/s11207-011-9834-2

Schou, J., Scherrer, P. H., Bush, R. I., et al. 2012, SoPh, 275, 229, doi: 10.1007/s11207-011-9842-2

Sharykin, I. N., & Kosovichev, A. G. 2020, ApJ, 895, 76, doi: 10.3847/1538-4357/ab88d1

Simnett, G. M. 1986, SoPh, 106, 165, doi: 10.1007/BF00161361

Stefan, J. T., & Kosovichev, A. G. 2020, ApJ, 895, 65, doi: 10.3847/1538-4357/ab88ae

—. 2022, ApJL, 937, L26, doi: 10.3847/2041-8213/ac8f92

Švanda, M., Jurčák, J., Kašparová, J., & Kleint, L. 2018, ApJ, 860, 144, doi: 10.3847/1538-4357/aac3e4

Švestka, Z. 1970, SoPh, 13, 471, doi: 10.1007/BF00153567

Wang, H., Ewell, M. W., J., Zirin, H., & Ai, G. 1994, ApJ, 424, 436, doi: 10.1086/173901

Zirin, H., & Tanaka, K. 1981, ApJ, 250, 791, doi: 10.1086/159429

Zvereva, A. M., & Severnyj, A. B. 1970, Izvestiya Ordena Trudovogo Krasnogo Znameni Krymskoj Astrofizicheskoj Observatorii, 41, 97